Khulna University Studies Special Issue ICSTEM4IR: 291-306, 2022

ORIGINAL ARTICLE

SCIENCE & ENGINEERING

NUMERICAL MODELLING OF A NON-LINEAR RADIATIVE NON-NEWTONIAN NANOFLUID FLOW WITH ARRHENIUS ACTIVATION ENERGY

Sk. Reza-E-Rabbi[1,*], Md. Yousuf Ali[1], S. M. Arifuzzaman[2], Md. Shakhaoath Khan[3], Sarder Firoz Ahmmed[1]

[1]Mathematics Discipline, Khulna University, Khulna- 9208
[2]Centre for Infrastructure Engineering, Western Sydney University, NSW-2751, Australia
[3]Department of Chemical and Biological Engineering, Monash University, VIC-3800, Australia

KUS: ICSTEM4IR-22/0013

Manuscript submitted: July 30, 2022 Accepted: September 26, 2022

Abstract

This research has examined the flow properties of non-linear radiative nano non- Newtonian fluid flow via a stretched sheet, as well as the impact of Arrhenius activation energy isalso inspected. The basic equations, which comprised time-dependent pivotal equations, were builtusing boundary layer approximations. As a numerical methodology, an explicit finite difference (EFD) technique was exerted. The fluid flow has been simulated employing FORTRAN in this case. A stability and convergence study has been performed to determine the accuracy of the numerical approach, and the system was determined to be converged at $Pr \geq 0.062$, and $Le \geq 0.016$. Here, non-dimensional outcomes based on various physical characteristics are considered. The effect of these numerous physical characteristics is explained and visually represented for a variety of flow fields. Furthermore, the examination of streamlines and isothermal lines has demonstrated enhanced visualization of the fluid flow. It has been revealed that non-linear pattern thermal radiation has a substantial impact on the heat transfer properties of nanofluid. Moreover, when non-linear radiation is addressed, the Lorentz force also has a significant impact on fluid flow. A great agreement has also served as a confirmation of the current effort. This sort of fluid has potential uses in mining, lubrication, and biomedical flow.

Keywords: Non-Newtonian fluid, MHD, Mass and heat transmission, non-linear radiation,Activation energy.

Introduction

At present, many researchers have investigated non-Newtonian nanofluid flow because of its vast applications in many chemical engineering and the food industry. Bhatti et al (2021) researched Arrhenius activation energy with thermo-bioconvection flow of nanofluid and the flow through a Riga plate. The impacts of magnetic field and the bioconvection Rayleigh number on velocity profiles, activation energy on concentration profiles and Brownian motion on temperature profiles have been investigated in their work. Alamri et al. (2019)

*Corresponding author: <rabbi06@math.ku.ac.bd >
DOI: https://doi.org/10.53808/KUS.2022.ICSTEM4IR.0013-se

investigated the plane Poiseuille radiative flow of nanofluid towards a porous medium with slip conditions. Homotopy analysis has been employed for obtaining the numerical solution and the influence of Stefan blowing has been described by graphically with short description. The influence of magnetic field on stagnation point with nonlinear radiation of nanofluid flow through a stretching sheet has been studied by Ghasemi et al. (2022). The reduction of temperature profiles caused by increasing the Prandtl number for different values of radiation parameter was the principal outcome of their work as well as the impressions of Lewis number on temperature profiles has been investigated. The study of heat generation and the influence of nonlinear radiation has been investigated by Akinshilo et al. (2021) and the Casson nanofluid flow has been embedded in the porous medium. Ullah et al. (2021) studied on effects of activation energy in a nanofluid flow, which was magnetized and the system was considered as rotating with an exponential heat source. For getting numerical simulations, NDSolve approach has been employed and they found that the rate of mass transformation has been decreased by increasing the activation energy. Kalaivanan et al (2020) researched the Arrhenius activation energy in a fluid flow with second-grade nanofluid including active and passive controls of the materials. In 2019, the study on hydrodynamic stability and heat transfer with the mass transfer of MHD radiative fluid with fourth-grade has been investigated by Arifuzzaman et al. (2019) in presence of chemical reaction through the porous plate. As the fluid grade increased, it was noticed that the velocity fields started to decrease, but when the temperature fields were looked at, the situation was completely the reverse. The influence of the grade of the fluid on velocity fields and temperature fields and it is found that the opposite nature of them. The advabced visualization of stream lines and isothermal lines have been described as the outcomes of the influence of thermal radiation. Reza-E-Rabbi et al. (2020a), studied multiphase nanofluid flow with computational modeling, where the fluid flow past a stretching sheet. The outcomes of their work have been described with the help of various graphical representation and the influence of various fluid related phenomena have been discussed separately. In 2020, Reza-E-Rabbi et al. (2020b), also researched unsteady MHD Casson nanofluid flow in presence of chemical reaction. Khan et al. (2020), investigated nanofluid flow with second law analysis where not only activation energy but also the binary chemical reaction were incorporated. Irfan et al. (2021) analyzed Carreau nanofluid flow with mass flux theory in presence of Arrhenius activation energy. Asllanaj et al. (2021) showed various formulations of the WSGC model and also discussed the numerical simulations of heat transfer in presence of radiation. The influence of chemical reactions on the MCCI model with the heat transfer process has been researched by Cao et al. (2022). In 2022, Mabood et al. showed the influence of non-linear radiation with the chemical reaction on nanofluid flow in presence of Oldroyed-B. Gopal et al. (2022) presented a numerical study on MHD nanofluid flow in presence of a first-order chemical reaction past an exponential stretching sheet. Many of the researchers also have researched non-Newtonian fluids in modern times to understand the vast implications of such fluids. For instance, see the folllowings [Reza-E-Rabbi et al. (2019, 2022), Rana et al. (2022), Bhatti et al. (2019), Prakash et al. (2019)].

Considering the above discussion and inspired by the applications of non-Newtonian fluid, this article has been designed. Reza-E-Rabbi et al(2020b) .'s work has indeed been elaborated upon here. They have left the inclusion of non-linear radiation and activation energy undone, which has been tested in this study. The research indicates that non-linear pattern thermal radiation has a significant influence on nanofluid heat transfer qualities. Another unique feature is that when non-linear radiation is considered, the Lorentz force has a considerable influence on fluid movement. The present project has been structured as follows:

- To formulate the flow-related boundary layer equations such as continuity, momentum, energy and concentration equations.
- To obtain the numerical solution the dimensional equations have been converted into non-dimensional equations with the help of appropriate dimensionless variables and parameters.
- The explicit finite difference (EFD) technique has been employed to get the numerical outcomes by using FORTRAN programing language.

- ❖ Different flow-related phenomena have been discussed graphically with a short summary.
- ❖ The comparison of nonlinear and linear radiation has been studied on several flow profiles such as velocity, temperature, streamlines and isothermal lines.

Materials and Methods

Governing equations

The conduction of non-Newtonian (Casson) unsteady nanofluid flow with non-linear radiation is inquired in presence of chemical reaction and Arrhenius activation energy through a porous medium. The fluid flow has been taken at the place $y=0$, while $u=U_0=\varepsilon x$ is the velocity with stretched (Figure 1). T_∞ and c_∞ are the wall temperature and concentration, respectively. In order to get the Casson term, the rheological equation can be taken as, (Vijaya et al. (2016))

$$\pi_{ij}=\begin{cases}\left(\mu_c+\dfrac{P_y}{\sqrt{2\pi}}\right)2\zeta_{ij} & when\ \ \pi>\pi_b\\ \left(\mu_c+\dfrac{P_y}{\sqrt{2\pi_b}}\right)2\zeta_{ij} & when\ \ \pi<\pi_b\end{cases}\qquad where,\ P_y=\mu_c\sqrt{2\pi}\lambda^{-1} \tag{1}$$

$$\therefore \upsilon'=\upsilon\left(1+\lambda^{-1}\right)\ \ where,\ \upsilon=\frac{\mu_c}{\rho} \tag{2}$$

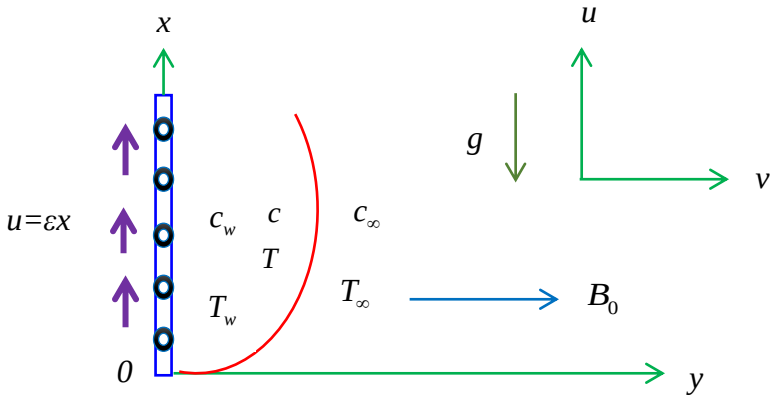

Figure 1. Physical configuration.

where, μ_c is the plastic dynamic viscosity of the Casson fluid, ζ_{ij} and π_{ij} are $(i,j)^{th}$ deformation rate and stress tensor, respectively. P_y indicates yield stress. From the above consideration and with the aid of the base idea of fluid mechanics and by following the work of Reza-E-Rabbi et al. (2020a) and Bhatti et al. (2021), we get the following Equations (3) to (6),

$$\frac{\partial u}{\partial x}+\frac{\partial v}{\partial y}=0 \tag{3}$$

$$\frac{\partial u}{\partial t}=\upsilon\left(1+\lambda^{-1}\right)\frac{\partial^2 u}{\partial y^2}+g\beta_C\left(c-c_\infty\right)-\sigma B_0^2\rho^{-1}u+g\beta_T\left(T-T_\infty\right)-\left(1+\lambda^{-1}\right)\frac{\upsilon u}{k_1}-\left(u\frac{\partial u}{\partial x}+v\frac{\partial u}{\partial y}\right) \tag{4}$$

$$\frac{\partial T}{\partial t}=\left(1+\lambda^{-1}\right)\frac{\upsilon}{c_p}\left(\frac{\partial u}{\partial y}\right)^2+\alpha D_T T_\infty^{-1}\left(\frac{\partial T}{\partial y}\right)^2+\alpha D_B\left(\frac{\partial c}{\partial y}\frac{\partial T}{\partial y}\right)-\left(\rho c_p\right)^{-1}\frac{\partial q_r}{\partial y}+\kappa\left(\rho c_p\right)^{-1}\frac{\partial^2 T}{\partial y^2}$$
$$-\left(u\frac{\partial T}{\partial x}+v\frac{\partial T}{\partial y}\right) \tag{5}$$

$$\frac{\partial c}{\partial t}=D_B\frac{\partial^2 c}{\partial y^2}-\sigma^2\left(c-c_\infty\right)^p\left(\frac{T}{T_\infty}\right)^n e^{\left(-E_a/kT\right)}+\frac{D_T}{T_\infty}\frac{\partial^2 T}{\partial y^2}-\left(u\frac{\partial c}{\partial x}+v\frac{\partial c}{\partial y}\right) \tag{6}$$

The initial boundary conditions are,

$$\left.\begin{aligned} &t=0,u=\varepsilon x,v=0,T=T_\infty,c=c_\infty \quad everywhere\\ &t\geq 0,u=0,v=0,T=T_\infty,c=c_\infty \quad at\ x=0\\ &u=\varepsilon x,v=0,T=T_w,c=c_w \quad at\ y=0\\ &u=0,v=0,T\to T_\infty,c\to c_\infty \quad at\ y\to\infty \end{aligned}\right\} \tag{7}$$

The approximation of Rosseland is depicted as, $q_r=-4\sigma'\left(3k^*\right)^{-1}\frac{\partial T^4}{\partial y}$. Then, the non-linear radiation term can be illustrated in the following way, $\frac{\partial q_r}{\partial y}=-16\sigma' T^3\left(3k^*\right)^{-1}\left(\frac{\partial^2 T}{\partial y^2}+T^2\left(\frac{\partial T}{\partial y}\right)^2\right)$. Thus, the energy equation turns into the given form,

$$\frac{\partial T}{\partial t}+u\frac{\partial T}{\partial x}+v\frac{\partial T}{\partial y}=\frac{\kappa}{\rho c_p}\frac{\partial^2 T}{\partial y^2}+\left(1+\lambda^{-1}\right)\frac{\upsilon}{c_p}\left(\frac{\partial u}{\partial y}\right)^2+\tau D_T T_\infty^{-1}\left(\frac{\partial T}{\partial y}\right)^2+\tau D_B\left(\frac{\partial c}{\partial y}\frac{\partial T}{\partial y}\right)$$
$$+16\sigma'\left(3k^*\rho c_p\right)^{-1}\left[T^3\frac{\partial^2 T}{\partial y^2}+T^2\left(\frac{\partial T}{\partial y}\right)^2\right] \tag{8}$$

The dimensionless variables for this fluid model are,

$$u=U_0U,\ v=U_0V,\ Y=\frac{yU_0}{\upsilon}\mathrm{Gr}^{1/4},\ X=\frac{xU_0}{\upsilon},\ \tau=\frac{tU_0^2}{\upsilon},$$
$$\theta=\frac{\left(T-T_\infty\right)}{\left(T_w-T_\infty\right)},\ \mathrm{T}=\left[1+\left(\theta_w-1\right)\theta\right]T_\infty,\ \theta_w=\frac{T_w}{\left(T_\infty\right)},c=\frac{\left(c-c_\infty\right)}{\left(c_w-c_\infty\right)} \tag{9}$$

Hence, the non-dimensional forms of the pivotal equations are,

$$\frac{\partial U}{\partial X}+\frac{\partial V}{\partial Y}=0 \tag{10}$$

$$\frac{\partial U}{\partial \tau}=\left(1+\lambda^{-1}\right)\frac{\partial^2 U}{\partial Y^2}+G_r\theta-MU+G_mC-\left(1+\lambda^{-1}\right)\phi U-\left(U\frac{\partial U}{\partial X}+V\frac{\partial U}{\partial Y}\right) \tag{11}$$

$$\frac{\partial\theta}{\partial\tau}=\frac{1}{\mathrm{P}_r}\left[1+Rn\left\{1+\left(\theta_w-1\right)\theta\right\}^3\right]\frac{\partial^2\theta}{\partial Y^2}+N_t\left(\frac{\partial\theta}{\partial Y}\right)^2\left(1+\lambda^{-1}\right)E_c\left(\frac{\partial U}{\partial Y}\right)^2+N_b\left(\frac{\partial C}{\partial Y}\frac{\partial\theta}{\partial Y}\right)$$
$$-\left(U\frac{\partial\theta}{\partial X}+V\frac{\partial\theta}{\partial Y}\right)+\left(\mathrm{P}_r\right)^{-1}Rn\left\{1+\left(\theta_w-1\right)\theta\right\}^3\left(\frac{\partial\theta}{\partial Y}\right)^2 \quad (12)$$

$$\frac{\partial C}{\partial\tau}=\left(L_e\right)^{-1}\frac{\partial^2C}{\partial Y^2}+N_t\left(N_b.L_e\right)^{-1}\frac{\partial^2\theta}{\partial Y^2}-Kr\left(\gamma\theta+1\right)^n\exp\left(\frac{-EA}{\gamma\theta+1}\right)C-\left(U\frac{\partial C}{\partial X}+V\frac{\partial C}{\partial Y}\right) \quad (13)$$

with

$$\left.\begin{aligned}&\tau\le 0,U=0,V=0,\theta=0,C=0 \quad everywhere\\&\tau>0,U=0,V=0,\theta=0,C=0 \quad at\ X=0\\&U=\varepsilon X=\varepsilon,V=0,\theta=1,C=1 \quad at\ Y=0\\&U=0,V=0,\theta=0,C=0 \quad as\ Y\to\infty\end{aligned}\right\} \quad (14)$$

Where, magnetic parameter $M=\frac{\sigma B_0^2\upsilon}{\rho U_0^2}$, Eckert number $E_c=\frac{U_0^2}{c_p\left(T_w-T_\infty\right)}$, Lewis number $L_e=\frac{\upsilon}{D_B}$, Prandtl number $P_r=\frac{\upsilon\rho c_p}{\kappa}$, temperature relative parameter $\gamma=\left(\frac{T_w-T_\infty}{T_\infty}\right)$, radiation parameter $Rn=16\sigma' T_\infty^3\left(3k^*\kappa\right)^{-1}$, Brownian motion parameter $N_b=\frac{\tau D_B\left(c_w-c_\infty\right)}{\upsilon}$, Arrhenius activation energy $EA=\frac{Ea}{kT_\infty}$, thermal Grashof number $G_r=\frac{\upsilon g\beta_T\left(T_w-T_\infty\right)}{U_0^3}$, thermophoresis parameter $N_t=\frac{\tau D_T\left(T_w-T_\infty\right)}{T_\infty\upsilon}$, porous term $\phi=\frac{\upsilon^2}{k_1U_0^2}$, mass Grashof number $G_m=\frac{\upsilon g\beta_c\left(c_w-c_\infty\right)}{U_0^3}$, chemical reaction $Kr=\frac{\upsilon\sigma^2}{U_0^2}$. Also the local friction factor, Nusselt number and Sherwood number can be described as,

$$Cf=-2.83\left(1+\lambda^{-1}\right)G_r^{-3/4}\left(\frac{\partial U}{\partial Y}\right)_{Y=0},\ Nu=0.71G_r^{-3/4}\left(\frac{\partial\theta}{\partial Y}\right)_{Y=0}\ \text{and}\ Sh=0.71G_r^{-3/4}\left(\frac{\partial C}{\partial Y}\right)_{Y=0} \quad (15)$$

The stream function ψ resolves continuity equation and the velocity component associated as, $U=\frac{\partial\psi}{\partial Y}$ and $V=-\frac{\partial\psi}{\partial X}$.

Numerical computation (explicit form)

We attempt to apply EFD technique for solving the obtained partial differential equation with corresponding to the boundary conditions. The height of the stretching sheet have been considered as X_{max} = 200 i.e. X changes from 0 to 200 and Y_{max} = 50 as resembling to $Y\to\infty$ i.e. Y varies from 0 to 50. For the axes grid spaces, we have to take m = 400 and n = 400 in the X- and Y- axes grid spaces (Figure 2).
Now by using explicit finite difference method we get,

$$\frac{U_{i,j}-U_{i-1,j}}{\Delta X}+\frac{V_{i,j}-V_{i,j-1}}{\Delta Y}=0 \tag{16}$$

$$U'_{i,j}=U_{i,j}+\left[\begin{array}{l}\left(1+\frac{1}{\lambda}\right)\frac{U_{i,j+1}-2U_{i,j}+U_{i,j-1}}{(\Delta Y)^2}+G_r\theta_{i,j}-MU_{i,j}+G_mC_{i,j}\\ -\left(1+\frac{1}{\lambda}\right)\phi U_{i,j}-U_{i,j}\left(\frac{U_{i,j}-U_{i-1,j}}{\Delta X}\right)-V_{i,j}\left(\frac{U_{i,j+1}-U_{i,j}}{\Delta Y}\right)\end{array}\right]\Delta\tau \tag{17}$$

$$\theta'_{i,j}=\theta_{i,j}+\left[\begin{array}{l}\frac{1}{P_r}\left[1+Rn\left\{(\theta_w-1)\theta_{i,j}\right\}^3\right]\left(\frac{\theta_{i,j+1}-2\theta_{i,j}+\theta_{i,j-1}}{(\Delta Y)^2}\right)+N_b\left(\frac{C_{i,j+1}-C_{i,j}}{\Delta Y}\frac{\theta_{i,j+1}-\theta_{i,j}}{\Delta Y}\right)\\ +\left(1+\frac{1}{\lambda}\right)E_C\left(\frac{U_{i,j+1}-U_{i,j}}{\Delta Y}\right)+N_t\left(\frac{\theta_{i,j+1}-\theta_{i,j}}{\Delta Y}\right)^2-U_{i,j}\frac{\theta_{i,j}-\theta_{i-1,j}}{\Delta X}-V_{i,j}\frac{\theta_{i,j+1}-\theta_{i,j}}{\Delta Y}\\ +\frac{1}{P_r}\left[Rn\left\{(\theta_w-1)\theta_{i,j}\right\}^3\right]\left(\frac{\theta_{i,j+1}-\theta_{i,j}}{\Delta Y}\right)^2\end{array}\right]\Delta\tau \tag{18}$$

$$C'_{i,j}=C_{i,j}+\left[\begin{array}{l}\frac{1}{L_e}\frac{C_{i,j+1}-2C_{i,j}+C_{i,j-1}}{(\Delta Y)^2}-U_{i,j}\left(\frac{C_{i,j}-C_{i-1,j}}{\Delta X}\right)-V_{i,j}\left(\frac{C_{i,j+1}-C_{i,j}}{\Delta Y}\right)\\ -Kr\left(\gamma\theta_{i,j}+1\right)^n\exp\left(\frac{-EA}{\gamma\theta_{i,j}+1}\right)C_{i,j}\end{array}\right]\Delta\tau \tag{19}$$

with

$$\left.\begin{array}{l}U_{i,o}^p=1,T_{i,o}^p=1,\mathrm{C}_{i,o}^p=1\\ U_{i,o}^p=0,\mathrm{T}_{i,\mathrm{L}}^p=0,\mathrm{T}_{i,\mathrm{L}}^p=0\ \text{where},L\to\infty\end{array}\right\} \tag{20}$$

Here, grid points with *X* and *Y* axes are symbolized by *i*, *j*, and *n*. Also, τ indicates time value, where $\tau=n\Delta\tau,n=1,2,3,.....$.

Stability and convergence analysis

To get the accuracy of the numerical solutions with finite difference method, it is mandatory to perform the analysis of the stability and convergence test. For actual mesh sizes, it is feasible to complete the stability test as the following way. Here, Equation (16) does not depend on Δt , so it can be neglected. It is considered that $e^{i\xi X}e^{i\psi Y}$ are the ordinary form of the Fourier expansion for *U*, θ and *C* at an arbitrary time $t = 0$, where $i=\sqrt{-1}$. At time *t*, the above terms become

$$U=P(t)e^{i\xi X}e^{i\psi Y}\ ;\ \theta=Q(t)e^{i\xi X}e^{i\psi Y}\ ;\ C=R(t)e^{i\xi X}e^{i\psi Y} \tag{21}$$

After a time step, these terms become as

$$U=P'(t)e^{i\xi X}e^{i\psi Y}\ ;\ \theta=Q'(t)e^{i\xi X}e^{i\psi Y}\ ;\ C=R'(t)e^{i\xi X}e^{i\psi Y} \tag{22}$$

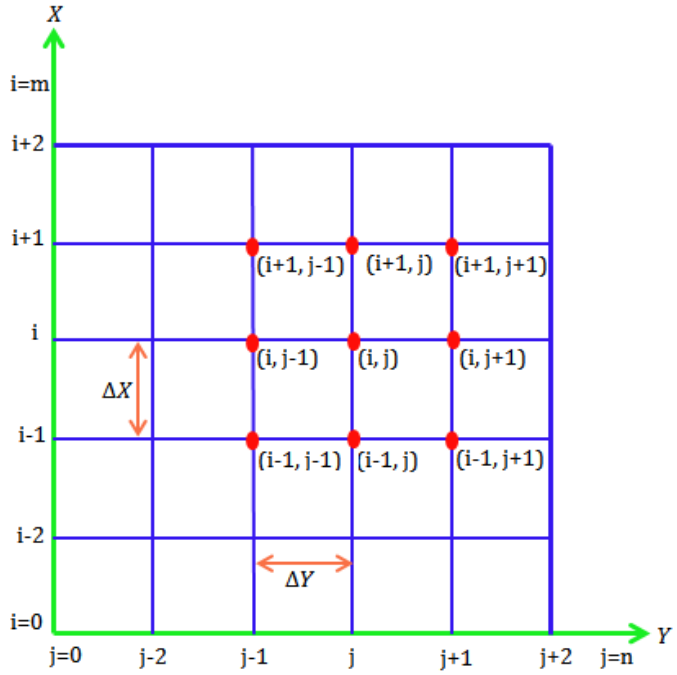

Figure 2. Finite difference grid spacing (Reza-E-Rabbi et al. (2022)).

Now by substituting the Equations (21) and (22) in Equations (17) to (19), we get

$$\frac{(P'-P)e^{i\xi X}e^{i\psi Y}}{\Delta\tau}=\left(1+\lambda^{-1}\right)\frac{2Pe^{i\xi X}e^{i\psi Y}\left(\cos\psi\Delta Y-1\right)}{\left(\Delta Y\right)^2}+GrQe^{i\xi X}e^{i\psi Y}+GmRe^{i\xi X}e^{i\psi Y}$$

$$-MPe^{i\xi X}e^{i\psi Y}-V\frac{P\left(e^{i\psi\Delta Y}-1\right)e^{i\xi X}e^{i\psi Y}}{\Delta Y}-U\frac{P\left(1-e^{-i\xi\Delta X}\right)e^{i\xi X}e^{i\psi Y}}{\Delta X}-\left(1+\lambda^{-1}\right)\phi Pe^{i\xi X}e^{i\psi Y}$$

$$P'=P[1+\left(1+\lambda^{-1}\right)\frac{2\left(\cos\psi\Delta Y-1\right)}{\left(\Delta Y\right)^2}\Delta\tau-V\frac{\left(e^{i\psi\Delta Y}-1\right)}{\Delta Y}\Delta\tau-U\frac{\left(1-e^{-i\xi\Delta X}\right)}{\Delta X}\Delta\tau]$$

$$+G_rQ\Delta\tau+G_mR\Delta\tau-MP\Delta\tau-\left(1+\lambda^{-1}\right)\phi P\Delta\tau$$

$$P'=A_1P+A_2Q+A_3R \tag{23}$$

Here,

$$A_1=1+[\left(1+\lambda^{-1}\right)\frac{2\left(\cos\psi\Delta Y-1\right)}{\left(\Delta Y\right)^2}-V\frac{\left(e^{i\psi\Delta Y}-1\right)}{\Delta Y}-U\frac{\left(1-e^{-i\xi\Delta X}\right)}{\Delta X}-M-\left(1+\lambda^{-1}\right)\phi]\Delta\tau \tag{24}$$

$$A_2=G_r\Delta\tau \quad ; \quad A_3=G_m\Delta\tau$$

$$\frac{(Q'-Q)e^{i\xi X}e^{i\psi Y}}{\Delta\tau}=\frac{1}{\mathrm{P}_r}\left[1+Rn\left\{1+(\theta_w-1)\theta\right\}^3\right]\frac{2Qe^{i\xi X}e^{i\psi Y}(\cos\psi\Delta Y-1)}{(\Delta Y)^2}$$

$$+N_b\frac{QR\left(e^{i\psi\Delta Y}-1\right)^2e^{2i\xi X}e^{2i\psi Y}}{(\Delta Y)^2}-V\frac{Q\left(e^{i\psi\Delta Y}-1\right)e^{i\xi X}e^{i\psi Y}}{\Delta Y}-U\frac{Q\left(1-e^{-i\xi\Delta X}\right)e^{i\xi X}e^{i\psi Y}}{\Delta X}$$

$$+N_t\left(\frac{Q\left(e^{i\psi\Delta Y}-1\right)e^{i\xi X}e^{i\psi Y}}{\Delta Y}\right)^2+\left(1+\lambda^{-1}\right)\left\{\frac{P\left(e^{i\psi\Delta Y}-1\right)e^{i\xi X}e^{i\psi Y}}{\Delta Y}\right\}^2$$

$$Q'=Q[(\Delta\tau)^{-1}+\frac{1}{\mathrm{P}_r}\left[1+Rn\left\{1+(\theta_w-1)\theta\right\}^3\right]\frac{2(\cos\psi\Delta Y-1)}{(\Delta Y)^2}+N_b\frac{C\left(e^{i\psi\Delta Y}-1\right)^2}{(\Delta Y)^2}-V\frac{\left(e^{i\psi\Delta Y}-1\right)}{\Delta Y}$$

$$-U\frac{\left(1-e^{-i\xi\Delta X}\right)}{\Delta X}+N_t\frac{\theta\left(e^{i\psi\Delta Y}-1\right)^2}{(\Delta Y)^2}+\frac{1}{P_r}\left[Rn\left(1+(\theta_w-1)\theta\right)^3\right]\frac{1}{(\Delta Y)^2}\left(e^{i\psi\Delta Y}-1\right)^2]\Delta\tau+\left(1+\lambda^{-1}\right)$$

$$U\frac{\left(e^{i\psi\Delta Y}-1\right)^2}{(\Delta Y)^2}P\Delta\tau$$

$$Q'=A_4P+A_5Q \tag{25}$$

Here,

$$A_4=\left(1+\lambda^{-1}\right)U\frac{\left(e^{i\psi\Delta Y}-1\right)^2}{(\Delta Y)^2}\Delta\tau$$

$$A_5=1+[\frac{1}{\mathrm{P}_r}\left[1+Rn\left\{1+(\theta_w-1)\theta\right\}^3\right]\frac{2(\cos\psi\Delta Y-1)}{(\Delta Y)^2}+N_b\frac{C\left(e^{i\psi\Delta Y}-1\right)^2}{(\Delta Y)^2}-V\frac{\left(e^{i\psi\Delta Y}-1\right)}{\Delta Y}$$

$$-U\frac{\left(1-e^{-i\xi\Delta X}\right)}{\Delta X}+N_t\frac{\theta\left(e^{i\psi\Delta Y}-1\right)^2}{(\Delta Y)^2}+\frac{1}{P_r}\left[Rn\left(1+(\theta_w-1)\theta\right)^3\right]\frac{1}{(\Delta Y)^2}\left(e^{i\psi\Delta Y}-1\right)^2]\Delta\tau \tag{26}$$

$$\frac{(R'-R)e^{i\xi X}e^{i\psi Y}}{\Delta\tau}=(Le)^{-1}\frac{2Re^{i\xi X}e^{i\psi Y}(\cos\psi\Delta Y-1)}{(\Delta Y)^2}+N_t(N_bLe)^{-1}\frac{2Qe^{i\xi X}e^{i\psi Y}(\cos\psi\Delta Y-1)}{(\Delta Y)^2}$$

$$-V\frac{R\left(e^{i\psi\Delta Y}-1\right)e^{i\xi X}e^{i\psi Y}}{\Delta Y}-U\frac{R\left(1-e^{-i\xi\Delta X}\right)e^{i\xi X}e^{i\psi Y}}{\Delta X}-Kr(\gamma\theta+1)^n\exp\left(\frac{-EA}{\gamma\theta+1}\right)Re^{i\xi X}e^{i\psi Y}$$

$$R'=R[(\Delta\tau)^{-1}+(L_e)^{-1}\frac{2(\cos\psi\Delta Y-1)}{(\Delta Y)^2}-V\frac{\left(e^{i\psi\Delta Y}-1\right)}{\Delta Y}-Kr(\gamma\theta+1)^n\exp\left(\frac{-EA}{\gamma\theta+1}\right)$$

$$-U\frac{\left(1-e^{-i\xi\Delta X}\right)}{\Delta X}]\Delta\tau+N_t(N_bL_e)^{-1}\frac{2Q(\cos\psi\Delta Y-1)}{(\Delta Y)^2}\Delta\tau$$

$$R'=A_6Q+A_7R \tag{27}$$

Here,

$$A_6 = N_t \left(N_b L_e\right)^{-1} \frac{2\left(\cos\psi\Delta Y - 1\right)}{\left(\Delta Y\right)^2} \Delta\tau$$

$$A_7 = 1 + [\left(L_e\right)^{-1} \frac{2\left(\cos\psi\Delta Y - 1\right)}{\left(\Delta Y\right)^2} - V \frac{\left(e^{i\psi\Delta Y} - 1\right)}{\Delta Y} - Kr\left(\gamma\theta + 1\right)^n \exp\left(\frac{-EA}{\gamma\theta + 1}\right) - U \frac{\left(1 - e^{-i\xi\Delta X}\right)}{\Delta X}]\Delta\tau \quad (28)$$

The Equations (23), (25) and (27) can be express as the matrix form

$$\begin{bmatrix} P' \\ Q' \\ R' \end{bmatrix} = \begin{bmatrix} A_1 & A_2 & A_3 \\ A_4 & A_5 & 0 \\ 0 & A_6 & A_7 \end{bmatrix} \therefore \eta' = A_M \eta \text{ where } \eta' = \begin{bmatrix} P' \\ Q' \\ R' \end{bmatrix}, \eta = \begin{bmatrix} P \\ Q \\ R \end{bmatrix} \text{ and } A_M = \begin{bmatrix} A_1 & A_2 & A_3 \\ A_4 & A_5 & 0 \\ 0 & A_6 & A_7 \end{bmatrix} \quad (29)$$

Due to the diversity of A_M, the study becomes quite difficult. As a result, a short time step has been taken i.e., $\Delta t \to 0$ and for this consideration we get $A_2 \to 0, A_3 \to 0, A_4 \to 0$ and $A_6 \to 0$. Hence,

$$A_M = \begin{bmatrix} A_1 & 0 & 0 \\ 0 & A_5 & 0 \\ 0 & 0 & A_7 \end{bmatrix} \quad (30)$$

The eigenvalues for the above matrix are $\lambda_1 = A_1, \lambda_2 = A_5$ and $\lambda_3 = A_7$, these data values must gratify the stability conditions which are given by the Equation (31)

$$|A_1| \le 1, \ |A_5| \le 1 \text{ and } |A_7| \le 1 \quad (31)$$

Again, let us consider

$$a = \Delta t, b = U \frac{\Delta t}{\Delta X}, c = |-V| \frac{\Delta t}{\Delta Y}, d = 2 \frac{\Delta t}{\left(\Delta Y\right)^2} \quad (32)$$

Here *a*, *b*, *c* and *d* are all real and non-negative values and also considering that the magnitudes of *U* and *V* are positive and negative, gradually. So, the maximum modulus of A_1, A_5 and A_7 can be obtained for $\xi\Delta X = m\pi$ and $\psi\Delta Y = n\pi$ with *m* and *n* are odd integer. Now by employing the Equations (33-35),

$$A_1 = 1 - 2[\left(1 + \lambda^{-1}\right)d + c + b + aM + a\left(1 + \lambda^{-1}\right)\phi] \quad (33)$$

$$A_5 = 1 - 2[\frac{1}{\mathrm{P}_r}\left[1 + 2Rn\left\{1 + \left(\theta_w - 1\right)\theta\right\}^3\right]d - N_b C d + c + b - N_t \theta d] \quad (34)$$

$$A_7 = 1 - 2[\left(L_e\right)^{-1} d + c + Kr\left(\gamma\theta + 1\right)^n \exp\left(\frac{-EA}{\gamma\theta + 1}\right) + b] \quad (35)$$

To gratifies the feasible values are $A_1 = -1$, $A_6 = -1$, $A_7 = -1$ and $A_9 = -1$. Thus, the stability ambience can be written as in Equation (36) and (37).

Moreover, the stability attributes of this problem are,

$$-\frac{2\Delta\tau}{\left(\Delta Y\right)^2} \frac{1}{P_r}\left\{1 + 2Rn\left(1 + \left(\theta_w - 1\right)\theta\right)^3\right\} + U\frac{\Delta\tau}{\Delta X} + V\frac{\Delta\tau}{\Delta X} - N_b \frac{2\Delta\tau}{\left(\Delta Y\right)^2} C - N_t \frac{2\Delta\tau}{\left(\Delta Y\right)^2}\theta \le 1 \quad (36)$$

$$U\frac{\Delta\tau}{\Delta X}+\frac{2\Delta\tau}{(\Delta Y)^2}\frac{1}{L_e}-\frac{\Delta\tau}{2}Kr\left(1+\gamma\theta\right)^n e^{\left(\frac{-EA}{1+\gamma\theta}\right)}-V\frac{\Delta\tau}{\Delta X}\le 1 \qquad (37)$$

Here, $U=0,V=0,\theta=0,C=0$ at $\tau=0$. For, $\Delta\tau$= 0.0005, ΔX= 0.20 and ΔY= 0.25, in this operation, the convergence criteria would be as follows: P_r≥0.062 and L_e≥0.016.

Results and Discussion

This portion has been designed with some graphical representation and short discussion of the outcomes of the problem. To get the numerical outcomes, the data of the following factors have been adopted as $G_r = G_m = \phi = \gamma = 1.00$, $\lambda = n = N_t = 0.50$, $M = EA = Rn = 2.00$, $Kr = N_b = 0.30$, $E_c = 0.01$, $L_e = 5.00$, $P_r = 0.71$, $\theta_w = 1.2$.

In Figure 3, it is observed that the decline of velocity because of increasing the amount of magnetic parameter M for both cases, i.e., the impacts of linear but also non-linear radiation. It is known that the magnetic field creates Lorentz force which treat as resistance, so the velocity profiles reduce with rises the magnetic parameters. But the velocity profiles can be seen that comparatively high for non-linear radiation to linear case. At Y = 2.00501 for the value of magnetic parameter M = 2, the velocity is 0.16851 with linear radiation while 0.17172 with non-linear radiation. The increasing of the velocity for non-linear radiation is 0.00321.

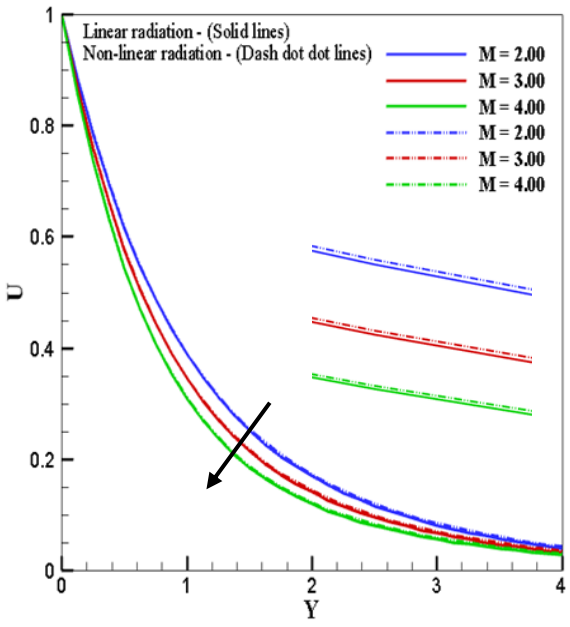

Figure 3. Impacts of M on velocity with linear and non-linear radiation.

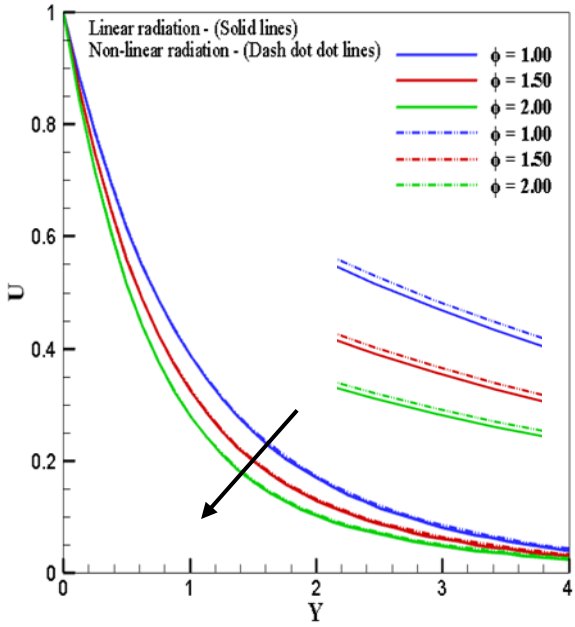

Figure 4. Impacts of ϕ on velocity for linear and non-linear radiation.

From Figure 4, it can be noticed that the dominance of porosity term on velocity and the velocity decreases with an increasing of the magnitudes of porosity parameter. But if we want to compare the velocity with respect to the radiation, it can be seen that the velocity with nonlinear radiation is more than linear radiation. The value of the velocity at Y = 1.00251 for ϕ = 1.00 with linear radiation is 0.38742 but for non-linear radiation the value is 0.38914 and the difference is 0.00172.

It is seen from Figure 5 the temperature increases as the results of the increasing of values Eckert number E_c for both conditions (linear radiation and non-linear radiation). If we noticed carefully, it can be watched that temperature profiles with non-linear radiation is elevated to linear radiation.

It can be noticed that from Figure 6, the nature of temperature with respect to Grashof number G_r and the improves of temperature profiles for both (linear radiation and non-linear radiation) facts. Though the temperature profiles are overhead in the sense of comparison between linear and non-linear radiation.

From Figure 7, the impact of chemical reaction parameter on concentration profile has been noticed and also seen that the concentration profiles reduce with rises the chemical reaction. It is also observed that the Arrhenius activation energy is more effective to increase the value of concentration with increasing the values of chemical reaction. The value of concentration with Arrhenius activation energy at $Y = 0.75188$ (for $Kr = 0.90$) is 0.48575 whereas in the absence of Arrhenius activation energy this velocity goes to 0.47975, where the decline concentration is 0.006.

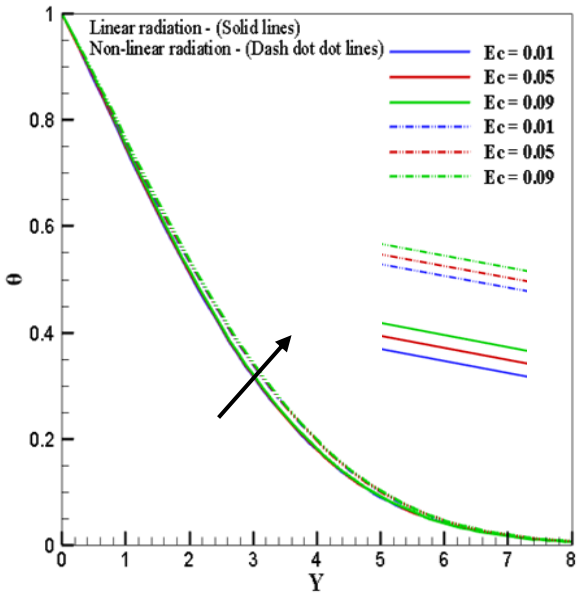

Figure 5. Nature of temperature due to change in E_c with linear and nonlinear radiation.

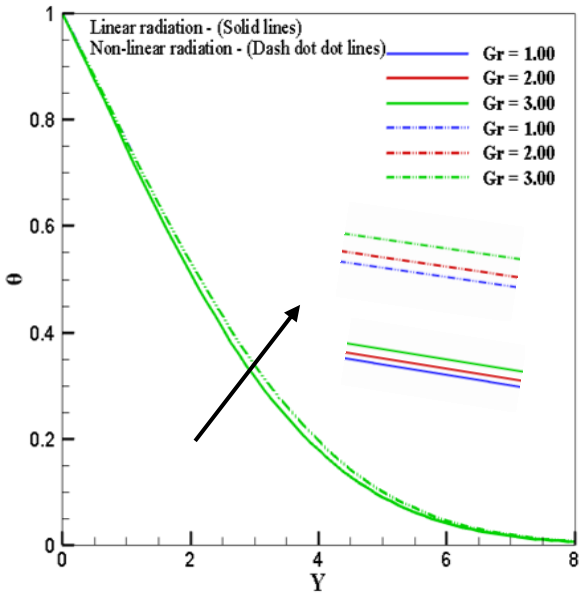

Figure 6. Nature of temperature due to change in G_r with linear and nonlinear radiation.

Figure 8 and Figure 9 represent the behavior of isothermal lines with the impact of Brownian parameter. Here, Figure 9 is the advanced visualization of the Figure 8 and from Figure 8 it can be observed that the increased of isothermal lines as the outcomes of the improvement of Brownian parameter. And also seen that the impression of radiation, whereas the isothermal lines with non-linear radiation is lofty to linear radiation.

Figure 10 and Figure 11 displayed the stream lines with changing thermophoresis parameter and here also be notable that the stream lines also increased by increasing the thermophoresis parameter isothermal lines. And it is also seen that with the presence of non-linear radiation (dashed dot lines), thermophoresis factor has upsurged the respective field dominantly rather than the linear one.

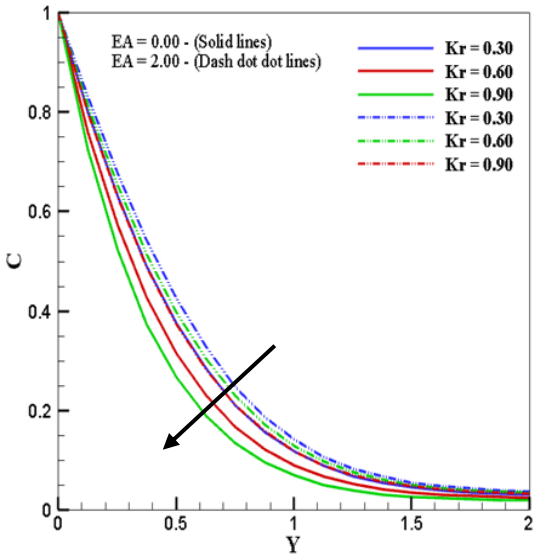

Figure 7. Variation of concentration because of *Kr* with and without Arrhenius activation energy, *EA*.

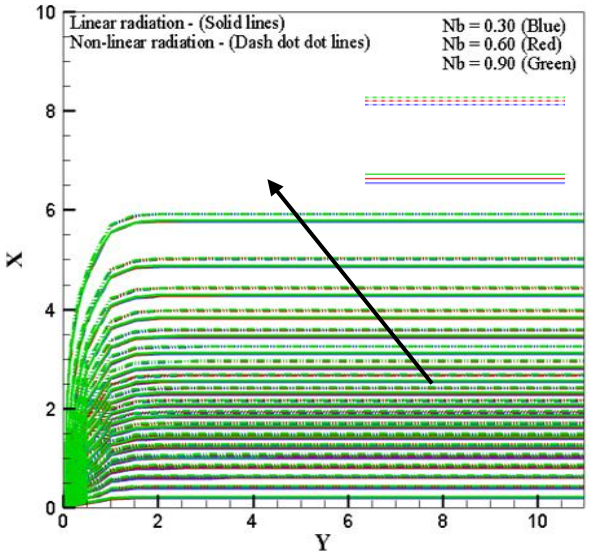

Figure 8. Nature of isothermal lines due to change in N_b with linear and non-linear radiation.

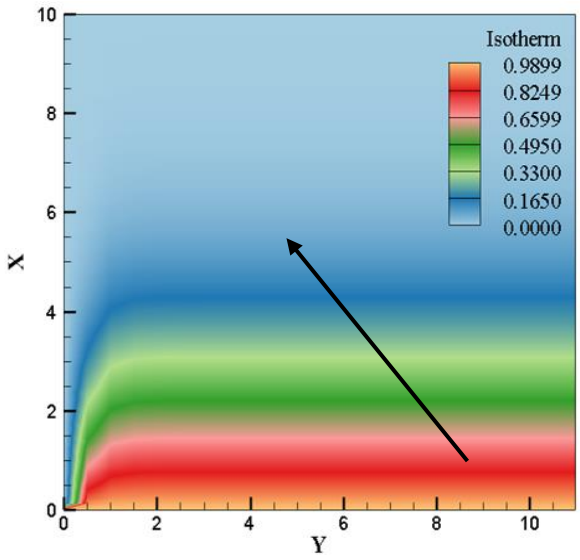

Figure 9. Advanced (Flood) view of Figure 8.

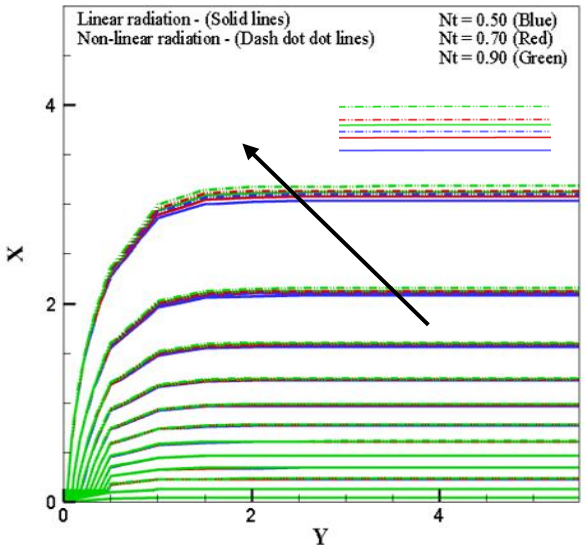

Figure 10. Nature of stream lines due to change N_t with linear and non-linear radiation.

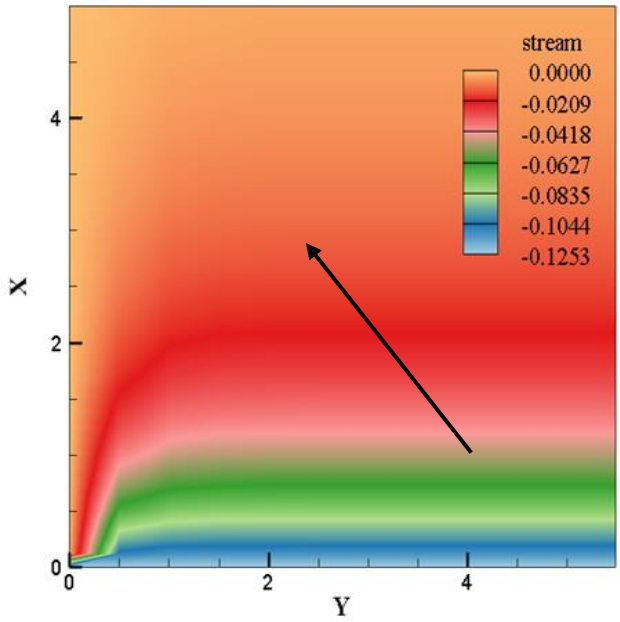

Figure 11. Advanced (Flood) view of Figure 10.

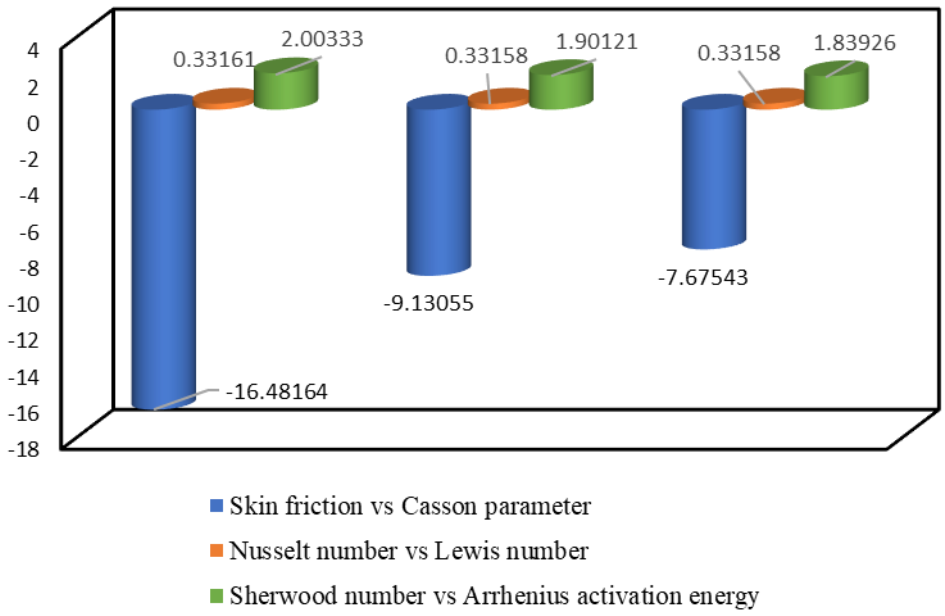

Figure 12. Mass plus heat transmission process at the wall for various factors.

Figure 12 deals some important physical phenomena such as skin friction against Casson parameter, Nusselt number against Lewis number and Sherwood number against Arrhenius activation energy and it can be seen that the skin friction increases while Sherwood number decreases though the Nusselt number decreases very few and after that it remains unchanged.

Validation

Figure 13 demonstrates a numerical assessment of the recent findings. The latest findings are in perfect agreement with Reza-E-Rabbi et al. (2019), who highlighted the percussion of linear radiation on Nusselt number, *Nu*. In this numerical validation (Figure 13), it is evident that for both cases, the Nusselt number, Nu increase with the acceleration of radiation factor and the numerical data of those studies have been found quite close to each other. This eventually renders the validation of the present research.

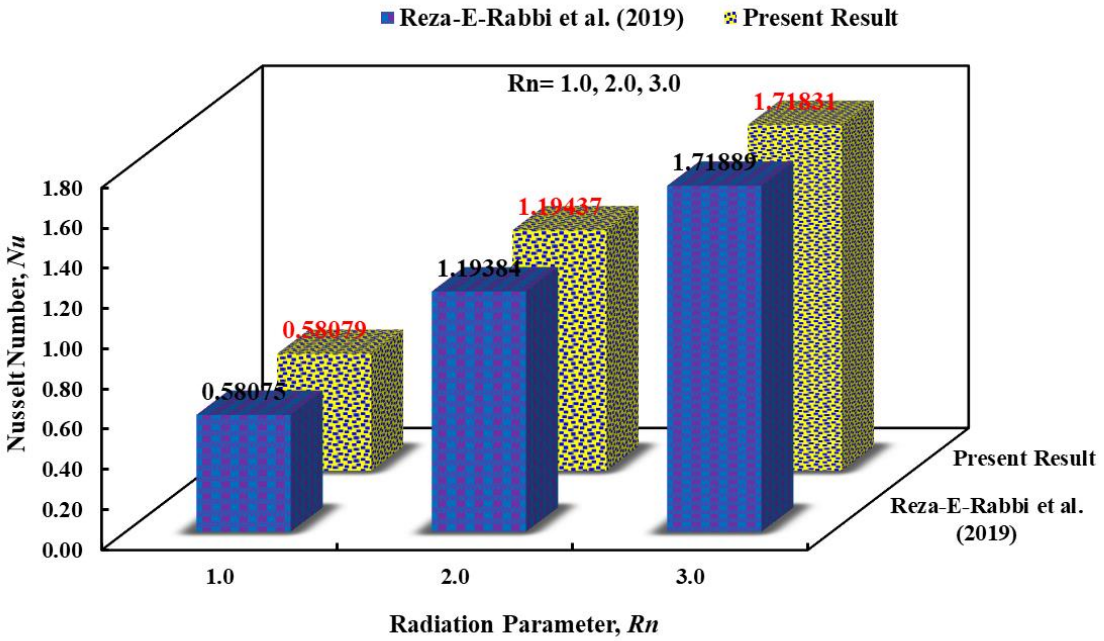

Figure 13. Numerical validation.

Conclusions

Here, heat but also mass transmission of nano non-Newtonian (Casson) liquid flow has been investigated numerically with the help of EFDM, incorporating the Arrhenius activation energy and nonlinear radiation as the investigation property. The principal outcomes of this research work are,

- As the increases of magnetic parameter and porosity term, the velocity profiles reduce for both cases i.e, linear or nonlinear radiation and the velocity is comparatively high for nonlinear radiation.
- The temperature has been enhanced because of the promting data of the Eckert number and Grashof number and also the value of the temperature is relatively high for nonlinear radiation.
- With the amplification of the value of chemical reaction parameter, the concentration profiles reduce for both cases i.e, with Arrhenius activation energy or without Arrhenius activation energy. But the

values of the concentration with activation energy is comparatively higher than without activation energy.

- The stream lines and isothermal lines are raising due to acceleration of the values of Brownian motion parameter and thermophoresis parameter respectively for both cases (linear and nonlinear radiation).
- An increase of the data of the Casson parameter, Lewis number and Arrhenius activation energy, the magnitudes of the skin friction, Nusselt number and Sherwood number has been prompted.

By incorporating phenomena such as exothermic/endothermic process, microorganisms, and so on, this theoretical analysis might be enlarged in the next days to any non-Newtonian fluids. Furthermore, experimental calculations can always reveal any theoretical judgment.

Acknowledgement

The authors appreciate the financial assistance provided by the Khulna University Research Cell. (KURC Grant, 2021) (ref no. KURC-04/2000-178 (খুবি/গসেল-০৪/২০০০-১৭৮)), Khulna University, Khulna-9208, Bangladesh.

References

Akinshilo, A. T., Mabood, F., & Ilegbusi, A. O. (2021). Heat generation and nonlinear radiation effects on MHD Casson nanofluids over a thin needle embedded in porous medium. *International Communications in Heat and Mass Transfer, 127, 105547.*

Alamri, S. Z., Ellahi, R, Shehzad, N., & Zeeshan, A. (2019). Convective radiative plane Poiseuille flow of nanofluid through porous medium with slip: an application of Stefan blowing. *J Mol Liq*, 273-292.

Arifuzzaman, S. M., Khan, M. S., Al-Mamun, A., Reza-E-Rabbi, S., Biswas, P., & Karim, I. (2019). Hydrodynamic stability and heat and mass transfer flow analysis of MHD radiative fourth-grade fluid through porous plate with chemical reaction. *Journal of King Saud University - Science*, 31(4), 1388-1398.

Asllanaj, F., Vivier, S. C., Botella, O., & Francis, H. R. (2021). França, Numerical solutions of radiative heat transfer in combustion systems using a parallel modified discrete ordinates method and several recent formulations of WSGG model, *Journal of Quantitative Spectroscopy and Radiative Transfer*, 274.

Bhatti, M. M., & Michaelides, E. E. (2021). Study of Arrhenius activation energy on the thermo-bioconvection nanofluid flow over a Riga plate. *J Therm Anal Calorim,* 143, 2029–2038.

Bhatti, M. M., Zeeshan, A., Ellahi, R., Beg, O. A. & Kadir, A. (2019). Effects of coagulation on the two-phase peristaltic pumping of magnetized Prandtl biofluid through an endoscopic annular geometry containing a porous medium. *Chinese J. Phys.* 68, 222–234.

Cao, Y., Lin, M., Shen M., & Li, J. (2022). Research on the influence of chemical reaction model over MCCI heat transfer process. *Annals of Nuclear Energy*, 165, 108793.

Ghasemi, S. E., Mohsenian, S., Gouran, S., & Zolfagharian, A. (2022). A novel spectral relaxation approach for nanofluid flow past a stretching surface in presence of magnetic field and nonlinear radiation, *Results in Physics,* 32, 105141.

Gopal, D., Jagadha, S., Sreehari, P., Kishan, N., & Mahendar, D. (2022). A numerical study of viscous dissipation with first order chemical reaction and ohmic effects on MHD nanofluid flow through an exponential stretching sheet. *Materials Today: Proceedings*.

Irfan, M., Rafiq, K., Khan, M., Waqas, M., & Anwar, M. S. (2021). Theoretical analysis of new mass flux theory and Arrhenius activation energy in Carreau nanofluid with magnetic influence. *International Communications in Heat and Mass Transfer*, 120, 105051.

Kalaivanan, R., Vishnu Ganesh, N., & Al-Mdallal, Q. M. (2020). An investigation on Arrhenius activation energy of second grade nanofluid flow with active and passive control of nanomaterials. *Case Studies in Thermal Engineering,* 22, 100774.

Khan, N.S., Kumam, P. & Thounthong, P. (2020) Second law analysis with effects of Arrhenius activation energy and binary chemical reaction on nanofluid flow. *Sci Rep* 10, 1226.

Khan, N. S. (2019). Influence of inclined magnetic field on Carreau nanoliquid thin film flow and heat transfer with graphene nanoparticles. *Energies* 12, 1459.

Khan, N. S. (2019). Mixed convection in MHD second grade nanofluid flow through a porous medium containing nanoparticle and gyrotactic microorganisms with chemical reaction. *Filomat* 33, 4627–4653

Khan, N. S. (2019). Study of two-dimensional boundary layer flow of a thin film second grade fluid with variable thermo-physical propertiesin three dimensions space. *Filomat* 33, 5387–5405.

Mabood, F., Abbasi, A., Farooq, W., Hussain, Z., Badruddin, I. A. (2022). Effects of non-linear radiation and chemical reaction on Oldroyd-B nanofluid near oblique stagnation point flow. *Chinese Journal of Physics*, 77, 1197-1208.

Prakash, J., Tripathi, D., Tiwari, A. K., Sait, S. M. & Ellahi, R. Peristaltic pumping of nanofluids through a tapered channel in a porous environment: Applications in blood flow. *Symmetry* 11, 868 (2019).

Reza-E-Rabbi, S., Ahmmed, S. F., Arifuzaman, S. M., Sarkar, T., & Khan M. S. (2020a). Computational modelling of multiphase fluid flow behaviour over a stretching sheet in the presence of nanoparticles. *Engineering Science and Technology, an International Journal*, 23(3), 605-617.

Reza-E-Rabbi, S., Arifuzzaman, S. M., Sarkar, T., Khan M. S., & Ahmmed, S. F. (2020b). Explicit finite difference analysis of an unsteady MHD flow of a chemically reacting Casson fluid past a stretching sheet with Brownian motion and thermophoresis effects. *Journal of King Saud University - Science*, 32(1), 690-701.

Reza-E-Rabbi, S., Arifuzzaman, S. M., Sarkar, T., Khan, M. S., & Ahmmed, S. F. (2019). Periodic magnetohydrodynamic simulation of Newtonian and non-Newtonian fluids flow behavior past a stretching sheet with nanoparticles. *AIP Conference Proceedings*, 2121(1), 070006.

Rana, B. M. J., Arifuzzaman, S. M., Islam, S., Reza-E-Rabbi, S., Hossain, K. E., Ahmmed, S. F., & Khan, M, S. (2022). Swimming of microbes in entropy optimized nano-bioconvective flow of Prandtl–Erying fluid. *Heat Transfer*, 1-35.

Reza-E-Rabbi, S., Khan, M. S., Arifuzzaman, S. M., Islam, S., Biswas, P., Rana, B. M. J., Al-Mamun, A., Hayat, T., & Ahmmed, S. F. (2022). Numerical simulation of a non-linear nanofluidic model to characterise the MHD chemically reactive flow past an inclined stretching surface. *Partial Differential Equations in Applied Mathematics*, 5, 100332.

Mabood, F., Abbasi, A., Farooq, W., Hussain, Z., Badruddin, I. A. (2022). Effects of non-linear radiation and chemical reaction on Oldroyd-B nanofluid near oblique stagnation point flow. *Chinese Journal of Physics*, 77, 1197-1208.

Ullah, I., Alghamdi, M., Xia, W.-F., Shah, S. I., & Khan, H. (2021). Activation energy effect on the magnetized-nanofluid flow in a rotating system considering the exponential heat source. *International Communications in Heat and Mass Transfer, 128, 105578.*

Vijaya, N., Sreelakshmi, K. & Sarojamma, G. (2016). Effect of Magnetic Field on the Flow and Heat Transfer in a Casson Thin Film on an Unsteady Stretching Surface in the Presence of Viscous and Internal Heating. *Open Journal of Fluid Dynamics*, 6, 303-320